SEASONAL INTEGRATIONS WITH REALISTIC BOUNDARY FORCING

Čedo Branković and Laura Ferranti

European Centre for Medium Range Weather Forecasts
Shinfield Park, Reading, United Kingdom

Abstract

A set of seasonal integrations with the ECMWF NWP model has been created in order to examine the potential of the model to simulate various aspects of atmospheric variability. In all experiments observed SSTs were used. For each season, over the period of five years (1986-1990), three integrations initiated on consecutive days were run. The predictability of seasonal time averages was studied. The model climatology for DJF and JJA seasons reproduces well all the major features of the large-scale circulation. However, in the DJF season the zonalization of extratropical flow reduces the amplitudes of planetary waves. In JJA the rainfall pattern is reasonably well simulated in most of the tropics, but low-level monsoon flow in the model is somewhat weaker than observed and associated rainfall amounts are too low.

The interannual variation of tropical large-scale flow is correctly captured. The variation of monsoon rainfall is also relatively well simulated, especially over the Sahel. However, in some regions (India) this is only a partial success. In the extratropics, interannual variability is well simulated providing the equatorial Pacific SST forcing is strong. The coherent and consistent model response to such a forcing is primarily seen in the Pacific/North American region. In other parts of the globe, the pattern and amplitude of model anomalies may vary. In the case of weak SST anomalies, the model response may differ even in the PNA region.

The model intraseasonal variability is assessed in terms of time-filtered fluctuations, frequency of blocking and frequency of circulation regimes. Whilst the distribution of model total variability compares well with the observed one, the contribution of various frequency bands to the total variance reveals disagreement over several locations. The simulated blocking frequency is quite realistic over the Atlantic/European region, however the maxima are displaced towards cooler underlying temperatures. Over the Pacific the simulated blocking frequency is a complete failure. Statistics of simulated weather regimes for the northern hemisphere wintertime circulation agrees reasonably well with the observed one.

The influence of various model formulations on seasonal integrations is assessed in terms of monsoon circulation and rainfall. It was found that the model with the adjustment convective scheme improves the dry bias over both the Sahel and India and the model with the semi-Lagrangian advection scheme improves rainfall rates over India.

The impact of initial data on the large-scale tropical flow is relatively small. Similar results are found for the rainfall over the Sahel, but not for India where rainfall amounts may be more dependent on initial conditions. In the extratropics, the model simulations with a weak anomalous boundary forcing indicate a relatively large variability due to initial conditions. On the other hand, strong SST anomalies in the runs from consecutive initial dates cause a consistent response over the PNA region. However, this is not the case in other parts of the globe.

The results support the notion that even on seasonal time scales multiple integrations may be required as a viable strategy to overcome the influence of inherent atmospheric instabilities.

1. INTRODUCTION

The theoretical limit of deterministic predictability (generally agreed to be about two weeks) and practical predictive skill (about one week) of current numerical weather prediction (NWP) models appear to restrict the use of dynamical models for predictive integrations on seasonal time scales. However, some studies (*Shukla*, 1981, for example) have shown that there is a scope for seasonal prediction, since large scale components of the flow remain predictable for longer periods, i.e. even beyond the limit of theoretical predictability. These components are found to be associated with slowly varying boundary forcings, like sea surface temperature (SST) anomalies or surface soil moisture. On the other hand, *Miyakoda et al.* (1983) have found that for a relatively longer time integrations a complex NWP models should be used, because only such models are able to simulate the multitude of interactions and feedbacks which take place on various spatial and time scales. Another non-negligible restrictive factor, a large computational demand associated with these integrations, has become less important because of the steady development of powerful supercomputers (*Bengtsson*, 1991).

Although dynamical seasonal forecasting has yet to be introduced in operational production, there is, at the moment, a number of centres performing these integrations in research mode (*WMO*, 1991). There are at least two reasons for that. Firstly, the idea of seasonal forecasting is normally associated with global coupled ocean-atmosphere general circulation models (GCMs). Before the full utilization of coupled models takes place it is extremely important to assess their potential. This is achieved in a relatively simple and straightforward way by mimicking part of the coupled system in which the atmospheric model is forced with observed SSTs, thus assuming a 'perfect' ocean model environment. (The potential of an ocean model is tested in a similar way by forcing the model with observed surface winds.)

Secondly, the need to assess the tendency of a GCM towards its own equilibrium state, the so called model climate drift, pushes the upper limit of integrations much further beyond the conventional time range of many operational models. Better understanding of model climate drift improves our knowledge of model systematic errors, especially in terms of the model's ability to correctly simulate low-frequency atmospheric variability.

Some of the results from a comprehensive dataset of seasonal simulations obtained by integrating a relatively recent version of the operational ECMWF NWP are presented. The dataset covers five years of seasonal experiments, thus enabling an assessment of interannual atmospheric variability in the model. Such an assessment has been carried out for both northern winter and summer, and during El Niño and La Niña events. The discussion concentrates mainly on the characteristics of large-scale flow and also, for some parameters, to regional scale patterns, where in particular the precipitation over monsoon areas is analysed. Since the dataset contains integrations initiated on consecutive dates, it was possible to address the problem of predictability and the influence of initial conditions on seasonal simulations. The model performance with respect to the frequency of blocking occurrences and with respect to the frequency of circulation regimes is discussed. Also, intraseasonal variability of the model for high, medium and low-frequency ranges is assessed. Additional experiments were performed with the aim of studying the impact of various model formulations on the seasonal time scale.

2. MODEL AND EXPERIMENTS

The experiment design discussed in this paper is different to that described in the study by *Palmer et al.* (1992), hereafter referred to as PBVM, where experiments with climatological SST were used as the reference. Also in PBVM an earlier version and lower horizontal resolution (T42) of ECMWF model was used. All the integrations discussed below were carried out with ECMWF cycle 36 model which was in the operational production from June 1990 to April 1991 (*Simmons et al.*, 1988; *Miller et al.*, 1992). The model resolution used in seasonal experiments was spectral T63 in the horizontal (compared to operational T106) and L19 in the vertical. The time range of experiments was about 120 days, depending on season and initial date. The initial dates were normally chosen on the first, second and third day of the month preceding calendar season. For example, the initial dates for June, July, August (JJA) runs were 1, 2 and 3 May and length of integrations were 122, 121 and 120 days respectively. The complete experimental dataset covers all seasons over the 5-year period, from MAM 1986 to DJF 1990/91.

During an integration the observed SST, obtained on an operational (quasi real-time) basis from the US National Meteorological Center (NMC) and interpolated to the ECMWF model grid, were updated every 5 days. The quality and amplitudes of anomalies in these analyses do not necessarily coincide with monthly averages which regularly appear in the NMC/CAC Climate Diagnostics Bulletin. The latter is normally a blend of observations collected in real-time and delayed mode (*Reynolds*, 1988).

The observed climate used in this study was derived as an average of ECMWF analyses over the period of 5 year, 1986 to 1990. Corresponding anomalies are defined as differences from such a 'climate'. The same approach is taken for the SST field as well, though much reliable long-term climate (*Reynolds and Roberts*, 1987) was available. However, in PBVM it was pointed out that an ambiguity may arise when comparing results based on a short-term climate derived from ECMWF analyses with results based on a long-term SST climate.

Fig. 1 demonstrates that SST anomalies in the equatorial Pacific derived from the short-term (5-year) climate are fairly representative of the anomalies based on the long-term climate. Similar agreement is found in the other parts of the world ocean, though the rather smooth nature of the long-term SST climate causes anomalies to have somewhat larger amplitudes than anomalies based on the short-term climate. Also, in Fig. 1 a clear interannual variability of both types of monthly anomalies is seen. The ENSO cycle had a weak signal in 1986 and changed to a strong warm anomaly in 1987. The La Niña peaked in 1988 and subsequently weakened in 1989 before finally turned into a weak El Niño in 1990. The amplitudes of short-term anomalies are systematically cooler than those calculated from long-term climatology. On average this difference in amplitude amounts to about 0.2 K indicating a relative warming of the equatorial Pacific waters in the period 1986-1990 in comparison with the past thirty years or so.

3. MODEL SEASONAL CLIMATE

The model results are presented in terms of seasonal rather than shorter time averages. With longer time averaging the proportion of inherent atmospheric variability decreases and the proportion of variability due to boundary forcing, e.g. SST anomalies, increases. This is becoming evident especially in the extratropics where natural fluctuations due to internal instabilities exist even under prescribed boundary conditions

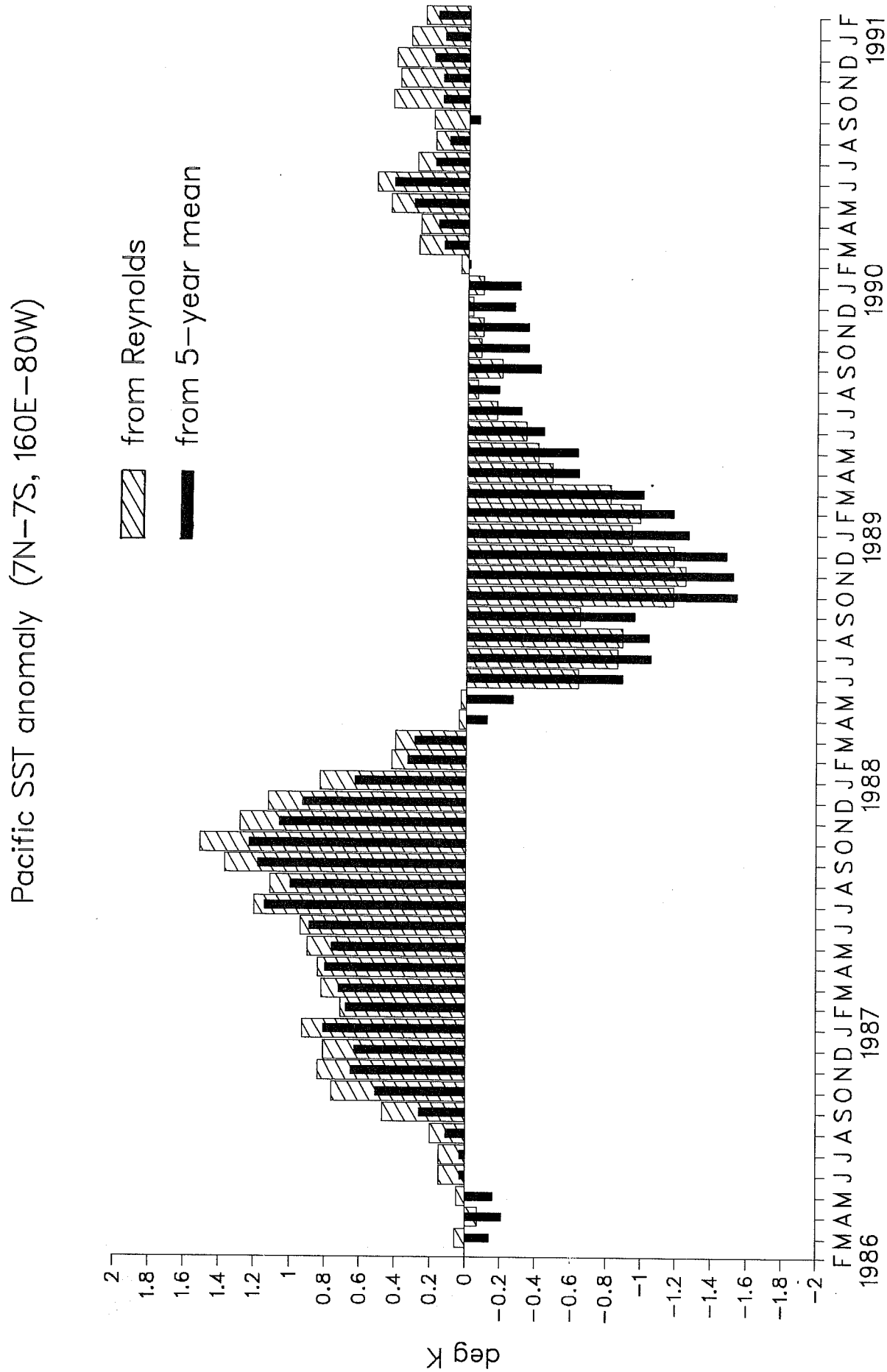

Fig.1 Monthly mean SST anomalies in the equatorial Pacific: hatched bars depict anomalies from Reynolds climatology, solid bars from 5-year average.

(*Palmer*, 1987). Thus, by looking into seasonal time averages we are able to extract from the experimental dataset a significant fraction of the signal due to SST forcing.

The model 'climate' was derived from 15 runs within a season (5 years times 3 experiments per year initiated 24 hours apart). It generally reproduces well the major large-scale circulation features in both DJF and JJA seasons. However, when compared with observed short-term climate (obtained as the averages over the 5-year period), some differences emerge in representing the details of the flow. Before focusing on the model's ability to typify observed interannual variability (in terms of anomalies derived with respect to model 'climate'), we briefly compare simulated against observed mean fields.

The model simulated 500 mb height field for the DJF season, averaged over 15 integrations, shows all the main features of the 5-year mean observed northern wintertime circulation (Fig. 2 a,b). The positioning of semi-permanent troughs over eastern continental seaboards and ridges over western seaboards is well represented. However, amplitudes of ridges and troughs are reduced indicating weakening of planetary waves in simulated flow. This well known zonalization of large-scale flow is seen as the typical negative/positive dipole structure in the error field over the north Pacific and north Atlantic regions (Fig. 2c). The zonalization implies a strengthening of the Pacific and Atlantic jets, and this is reflected in a strengthening of surface subtropical highs to the southeast of these jets. The positioning of Icelandic and Aleutian surface lows is well simulated, i.e. they have not drifted too far downstream as in earlier ECMWF models (not shown).

In the southern hemisphere the error distribution is to a certain extent similar to that in the northern hemisphere, i.e. negative errors are found poleward and positive equatorward of the polar jet (around 60°S), indicating a too strong circumpolar vortex in model simulations. This error is larger over the southern oceans than over the southern continents.

In the tropics, the mean monsoon flow at 850 mb over the Arabian sea is weaker in the model than the observed (Fig. 3 a,b) and also pushed too far north over the south Asia. The lee wave feature in the flow over southern India and the Bay of Bengal is represented in the model by a broad diffluent flow. In the Indian ocean, the modelled easterlies have too strong southerly component. This model bias, associated with too strong convergence in the equatorial region, will be discussed in the section on the impact of various model formulations on monsoon flow.

Away from the monsoon region, the model tends to overestimate the low-level wind from the Atlantic into South America and produces the spurious and substantial convergence over Central America. At 200 mb the easterlies over north Indian ocean are weaker in the model than observed (not shown).

Fig. 4 a,b shows how well the model mean tropical rainfall for JJA season compares with the climate (*Jaeger*, 1976). The model predicts less rainfall over the Sahel and India (Fig. 4b). For example, Lake Chad in Africa lies to the north of the 1 mm/day contour in simulated field, whereas in the observed climate it is south of the 4 mm/day contour. This is consistent with the results of PBVM, who found that the T42 model tends to underestimate the rainfall amounts in monsoon regions. However, whilst the dry bias may be blamed for insufficient rainfall amounts over India, this must be taken with some caution over the Sahel. Rather low rainfall rates over the Sahel shown in Fig. 4b may also reflect the natural climate trend from normal in mid-

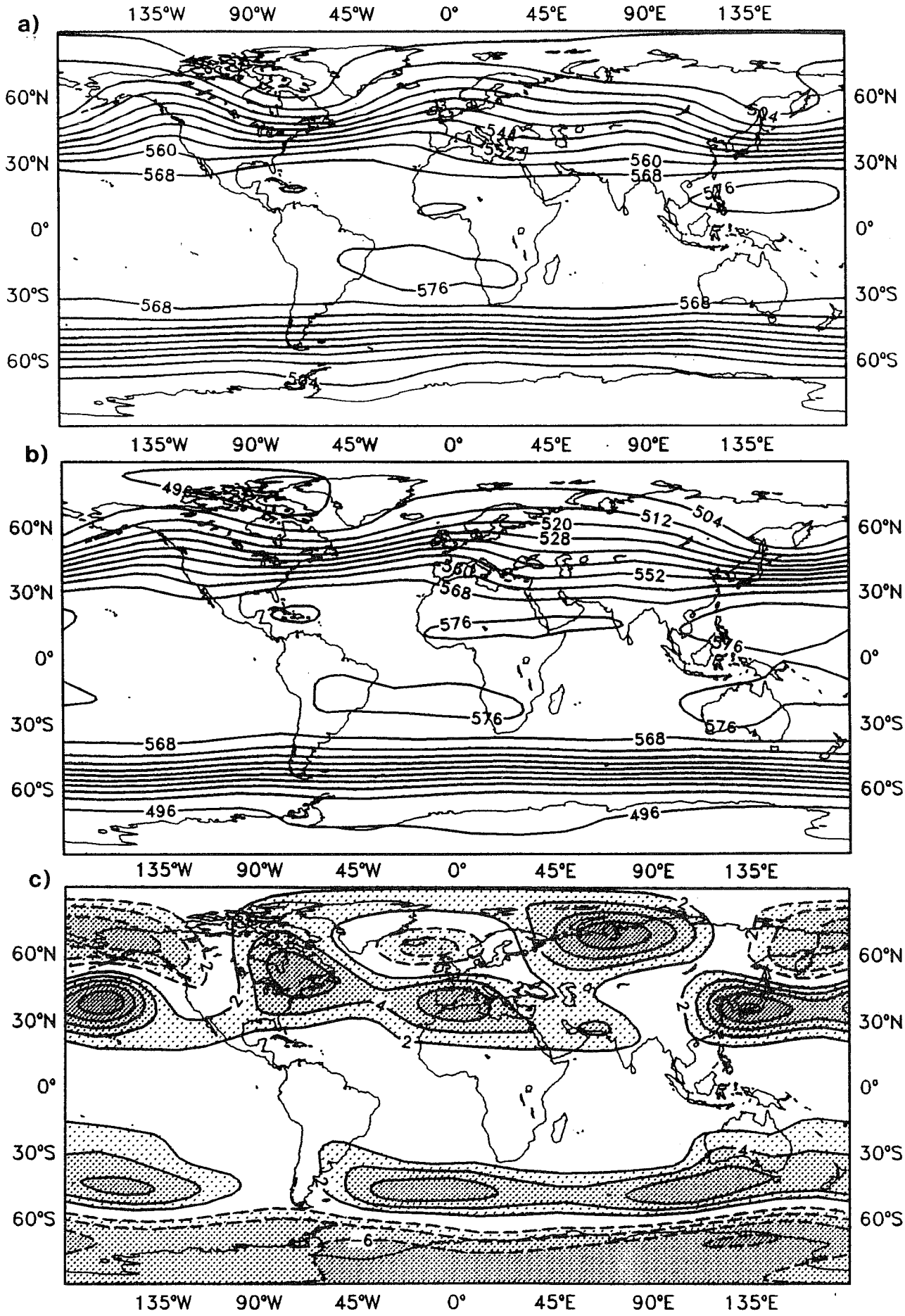

Fig.2 Mean DJF 500 mb heights: a) observed climate (5-year mean), b) model climate (from 15 runs), c) model error (difference b) minus a)). Contours every 8 dam in a) and b) and every 2 dam in c).

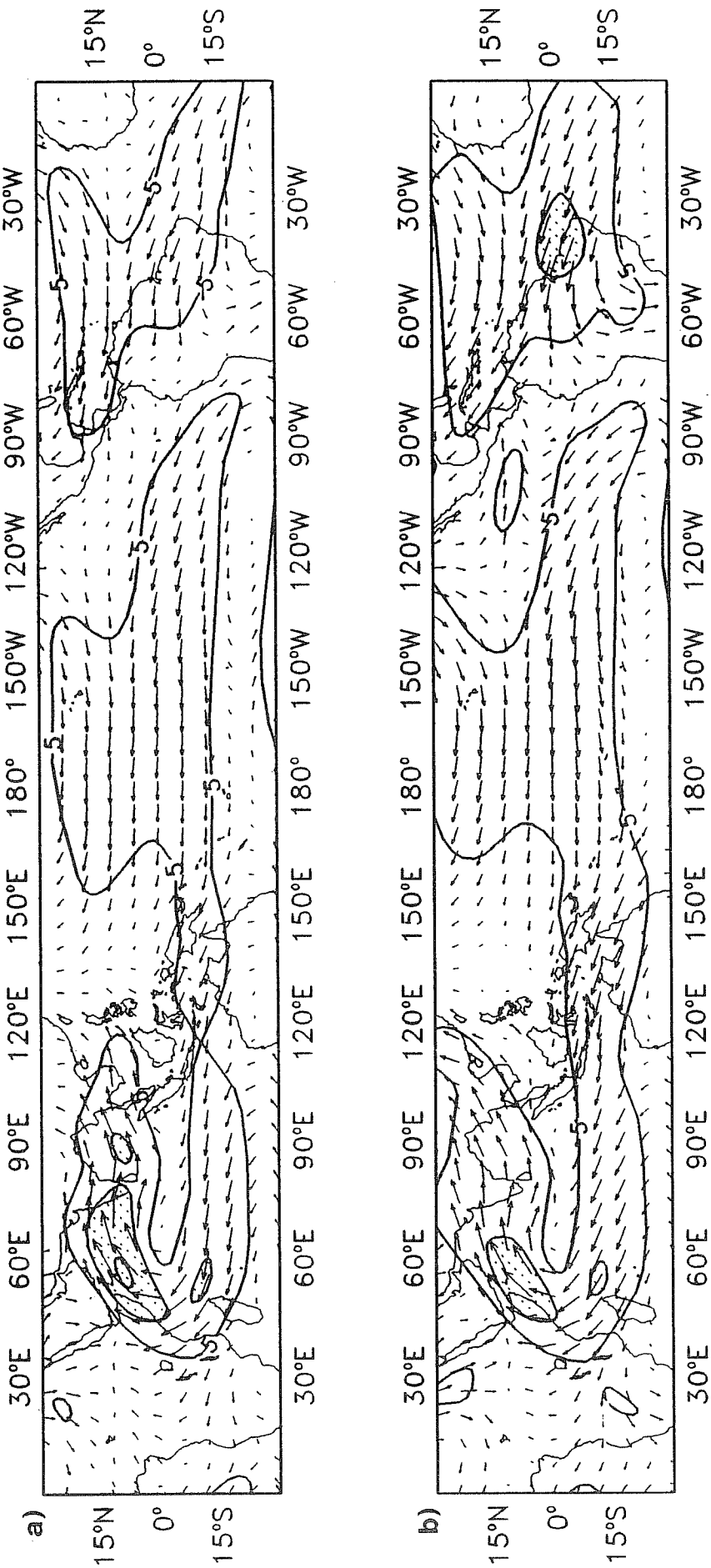

Fig.3 Mean JJA 850 mb tropical wind: a) observed climate, b) model climate. Contours every 5 ms^{-1}.

Fig.4 Mean JJA tropical rainfall: a) Jaeger (1976) climate, b) model climate, c) mean operational short-range forecast. Contours 1, 2, 4, 8, 12, 16, 20, ... mmday^{-1}.

1960s towards exceptionally dry years in 1980s (*Nicholson*, 1985). This trend is not taken into account in the Jaeger data because his climate was derived from the observations dated before 1960s.

Perhaps, a more meaningful reference for Fig. 4b might be the ECMWF operational short-range rainfall forecast (36 hours minus 12 hours; Fig. 4c) averaged for the same period JJA 1986-1990. *Arpe* (1990) found that the short-range forecast gives a relatively good approximation of tropical rainfall when compared with the estimates derived from observational OLR data. The comparison of rainfall over the Sahel from Fig. 4b and Fig. 4c still indicates too low values in our seasonal runs, however, not so dramatic as when compared with the Jaeger climatology.

The other apparent differences between Fig. 4b and either reference field are found over Central America, off the coast of South America and over the Indian ocean, where seasonal simulations overestimate JJA rainfall. In the rest of the tropics, including the ITCZ and SPCZ regions, simulated seasonal rainfall compares reasonably well with climate and mean short-range forecast.

4. SIMULATION OF INTERANNUAL VARIABILITY

Interannual variability of various atmospheric fields in both tropics and extratropics will be discussed in terms of anomalies induced by strong and opposite SST anomaly forcing in the equatorial Pacific, El Niño and La Niña respectively (see Fig. 1). The model anomaly for a single season is defined as the difference between the ensemble mean (i.e. the average of three individual runs for the same season) and the model climate. In the section on predictability we shall discuss some individual model experiments.

4.1 Tropical large-scale flow

Fig. 5 shows observed and simulated 200 mb wind anomalies for seasons DJF 1986/87 and DJF 1988/89. In DJF 1986/87 (El Niño year), both observed and simulated anomalies (Fig. 5 a,b) qualitatively agree with the results from linear model studies (*Gill*, 1980). The positive SST anomaly in the equatorial Pacific in DJF 1986/87 plays the role of the low-level heat source. The response of the upper-air atmosphere to such a forcing is given by a pair of anticyclones on either side of the equator. The simulated anomaly resembles remarkably well the observed one, with stronger and better defined anticyclonic circulation in the southern than in the northern hemisphere.

The opposite circulation structure to that in Fig. 5 a,b is found in the La Niña year, DJF 1988/89 (Fig. 5 c,d), when the atmospheric response to a negative SST anomaly (anomalous cooling) is represented by a pair of upper-air anomalous cyclones. The simulated vortices are rather elongated in the east-west direction when compared with the analysed ones having stronger winds in the southern hemisphere. However, the overall agreement between Fig. 5c and Fig. 5d is rather good. These results confirm the usefulness of linear models in studying thermal forcing of tropical flow.

In Fig. 6, the difference in 200 mb velocity potential between the JJA 1988 (La Niña) and JJA 1987 (El Niño) is shown. It can be seen that this representative of large-scale upper-air divergence is relatively well simulated by the model (Fig. 6b). The positive values over the Pacific indicate the strengthening of upper-air convergence in JJA 1988, consistent with reduced low-level heating. This results in an overall intensification of the Walker circulation.

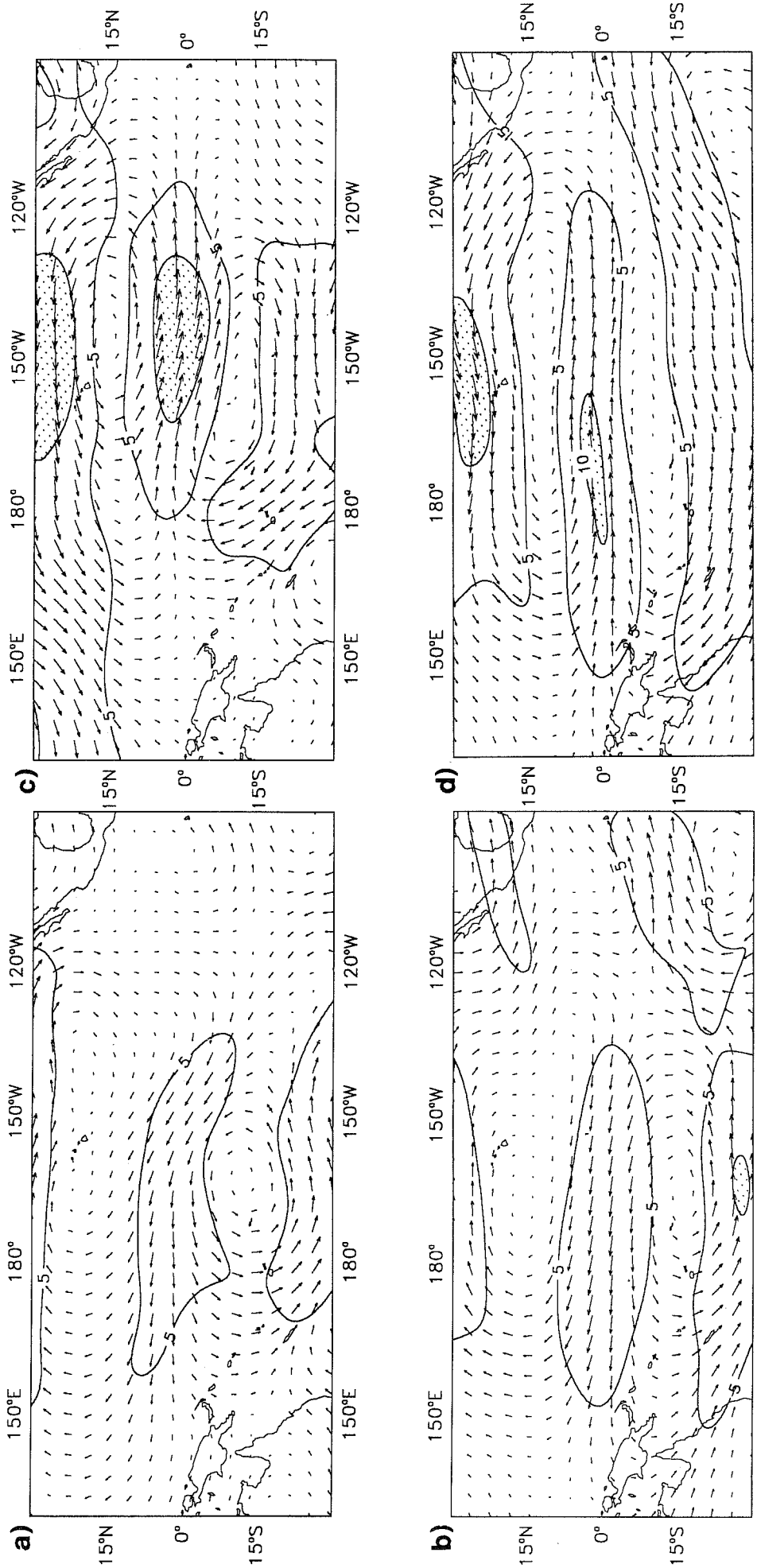

Fig.5 Mean DJF 200 mb wind anomaly: a) observed 1986/87, b) model mean 1986/87, c) observed 1988/89, d) model mean 1988/89. Contours every 5 ms^{-1}.

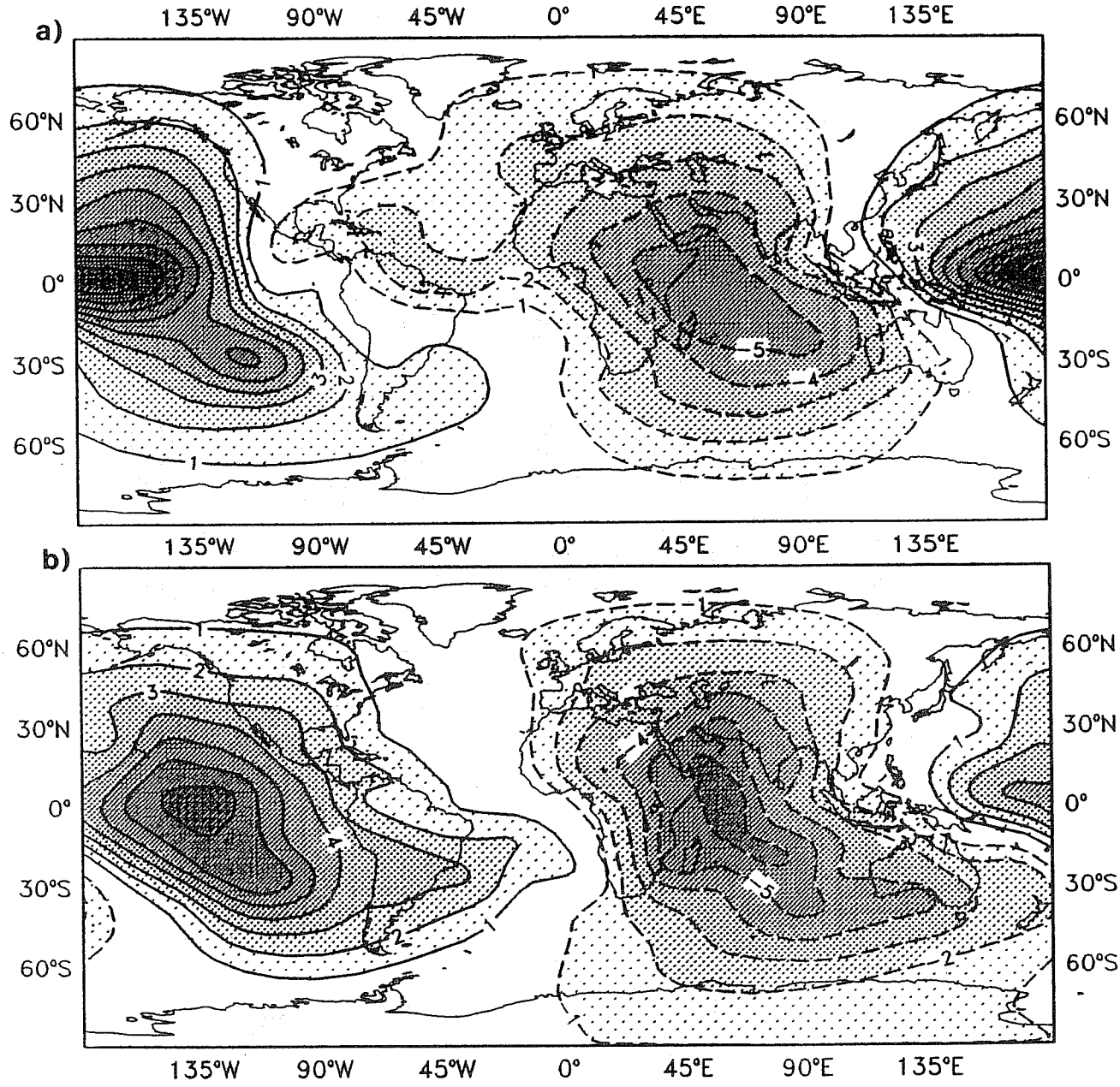

Fig.6 Mean JJA 200 mb velocity potential (χ) difference between 1988 and 1987: a) observed, b) model. Contours every 1×10^6 $m^2 s^{-1}$.

Over the Indian ocean the observed negative values denote an increase in upper-air divergence in JJA 1988. Such a differential velocity potential pattern is well captured by the model. This feature is the dominant contributor to interannual variability of simulated monsoon rainfall because of relatively little variation in model generated low-level flow from JJA 1987 to JJA 1988 (not shown).

4.2 Monsoon rainfall

It is well documented that JJA 1987 was a poor monsoon season in both the Sahel and most of India, and in JJA 1988 rainfall returned to normal conditions (see, for example, PBVM for the discussion on observational data). This natural fluctuation is relatively well reproduced in terms of simulated rainfall anomalies over the Sahel, but not so successfully over India (Fig. 7). In JJA 1987 (Fig. 7a) a coherent and well defined negative anomaly of about 1 mm/day stretches along about 12°N from western Africa into the Ethiopian highlands. The rainfall deficit affects mostly the southern part of the Sahel and the maximum is found along the coast of the Gulf of Guinea. A relatively southerly positioning of the Sahelian negative anomalies may be explained by the too dry climate of the model over the Sahel as discussed above and shown in Fig. 4b.

The poor monsoon in India is seen only as a small area of negative rainfall anomaly in the south of the subcontinent. The negative anomalies in the northeast appear to be wrong, because this part of India received in JJA 1987 more rain than normal (the opposite to the rest of the country).

The blank area over most of the Sahel in Fig. 7b represents a return to the normal rainfall conditions in JJA 1988. The positive anomaly over the Ethiopian mountains corresponds to excessive rainfall which caused devastating floods in Sudan. Over southern India, the positive anomaly is seen as an indicator of a good monsoon season, whilst positive anomalies around the Bay of Bengal indicate overestimated model rainfall, i.e. the model simulation again failed here.

4.3 Interannual variability in the extratropics

The teleconnection response of the extratropical atmosphere to the tropical SST anomaly forcing has been the subject of a number of studies (see, for example, *Horel and Wallace*, 1981). It was found that the Pacific/North American (PNA) region is 'preferred' in the sense that persistent upper-air atmospheric anomalies induced by strong anomalous SSTs tend to be located over that region. The positive PNA teleconnection pattern (negative height anomalies over the north Pacific and Atlantic and positive height anomaly over North America) is generally associated with the El Niño SST anomaly, whilst the negative PNA pattern is found to be associated with the La Niña forcing.

In Fig. 8a the difference in observed 500 mb heights between DJF 1986/87 (El Niño) and DJF 1988/89 (La Niña) is shown. A well defined wavetrain structure emerges over the PNA region. This structure is typical of a positive PNA teleconnection pattern, however, with much stronger amplitude. Large differences are also found over Europe and Asia as well as over the polar region. In the southern hemisphere a wavenumber 3 pattern is seen.

The ensemble mean difference between the two years for model simulated 500 mb heights is shown in Fig. 8b. In the northern hemisphere the PNA wavetrain is well established and dominant, indicating a relatively correct level of model sensitivity to imposed anomalous SST forcing. The amplitude of differences is somewhat weaker over North America and the Atlantic and much damped over the Asian continent and

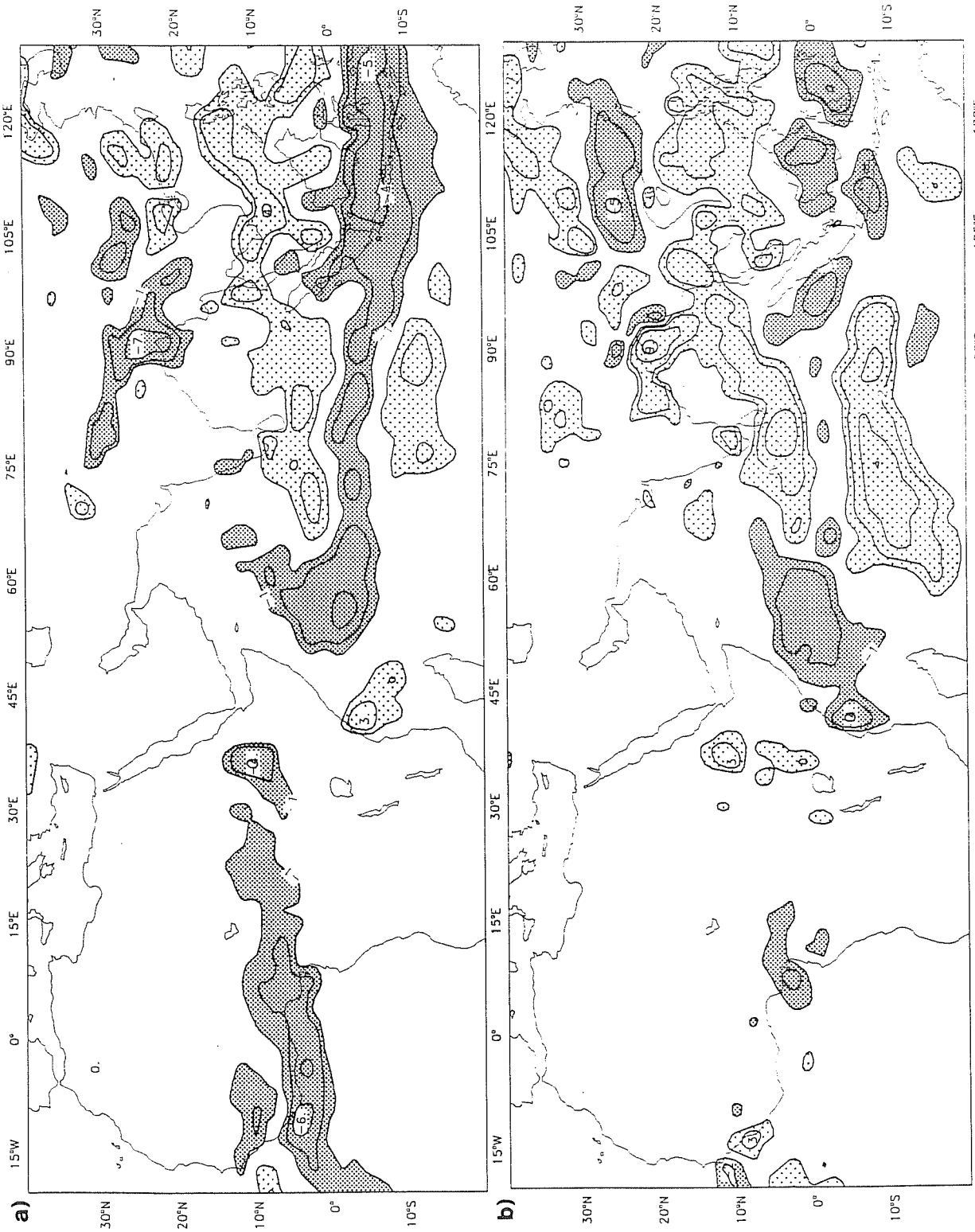

Fig.7 Mean JJA model rainfall anomaly for a) 1987 and b) 1988. Contours at ±1, ±2, ±4, ±8 and ±12 mmday^{-1}. Negative anomaly dense stippling, positive anomaly coarse stippling.

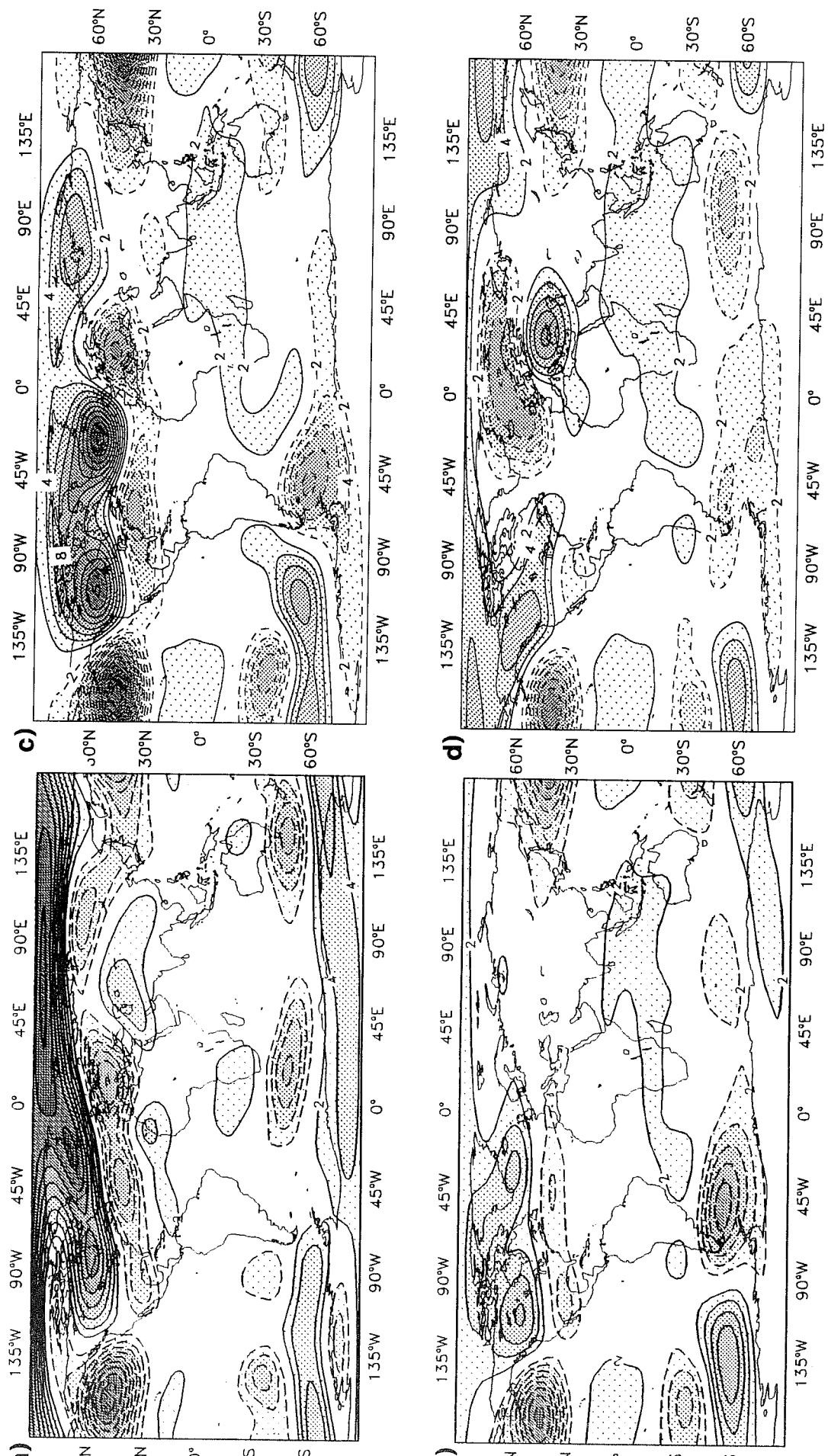

Fig.8 Mean DJF 500 mb height differences between 1986/87 and 1988/89 for a) observed b) model ensemble mean, c) experiments from 2nd November and d) experiments from 3rd November. Contours every 2 dam.

in the polar region. This weakening in amplitude away from the Pacific is a consequence of the opposite model responses in some of individual experiments with the El Niño SST anomaly. Fig. 8 c,d shows model 500 mb height differences between DJF 1986/87 and DJF 1988/89 for the two individual runs, one initiated on 2 November (Fig. 8c) and one initiated on 3 November (Fig. 8d). In both difference maps the PNA wavetrains are of the same structure, i.e. the positive PNA teleconnection pattern (though of different amplitudes). In the northern hemisphere high latitudes, away from the PNA region, differences are, however, of the opposite sign and relatively similar amplitudes. When the ensemble averaging is applied the overall effect of these differences is cancelled yielding in a weak difference in Fig. 8b.

5. SIMULATION OF INTRASEASONAL VARIABILITY

5.1 Time-filtered fluctuations

In order to assess the model variability on different time scales in midlatitudes, the standard deviation of DJF 500 mb heights has been computed for three different frequency ranges: high frequency (HF) with the period shorter than 10 days, medium frequency (MF) with the period between 10 and 30 days and low frequency (LF) with the period longer than 30 days. The standard deviation was calculated with respect to each annual mean, therefore it gives an estimate of variability within a season, excluding interannual fluctuations.

Fig. 9 left column shows the total standard deviation and the three partitions for the analysed DJF 500 mb heights averaged over the 5-year period, 1986/87-1990/91. The right hand side column shows the same fields averaged over 15 model DJF integrations. The total model variability (Fig. 9e) has almost the same geographical distribution as the observed one (Fig. 9a), although the maxima are underestimated - in particular over the Atlantic where the difference amounts up to 35 m. As discussed below, contributions of various frequency bands to the total variability differ in some areas for the model from those for the analysis.

The HF part of the standard deviation (Fig. 9 b and f) represents locations of jet streams and major storm tracks. In the model, the Pacific storm track penetrates too deeply into the North America and consequently the maximum variability is shifted downstream. The location of the Atlantic maximum is well captured in model simulations but the amplitude is slightly weaker than the observed. The simulated eastern branch of the Atlantic/European HF variability does not extend far enough into the Asian continent.

In the MF (Fig. 9 c and g) the maximum values of the variability coincide with locations of blocking. In comparison with the analysis, the model MF variability in the Pacific region is underestimated in both geographical extension and in magnitude (see also discussion in section 5.2). Over the Atlantic/European region the model MF variability is comparable with the observed one. The north Asian maximum is completely missed in the model.

The LF part of the midlatitude variability (Fig. 9 d and h) defined by fluctuations longer than 30 days contains the variability induced by seasonal cycle and possibly by low-frequency waves from the tropics (like 30-60 day oscillation). In the analysis two maxima of the LF variability are located at 60°N, one over the Alaskan coast and the other north of the British Isles. The model also shows these two maxima, however the one over the Pacific has a larger amplitude and geographical extension than its observed counterpart and the Atlantic one is weaker and displaced eastward.

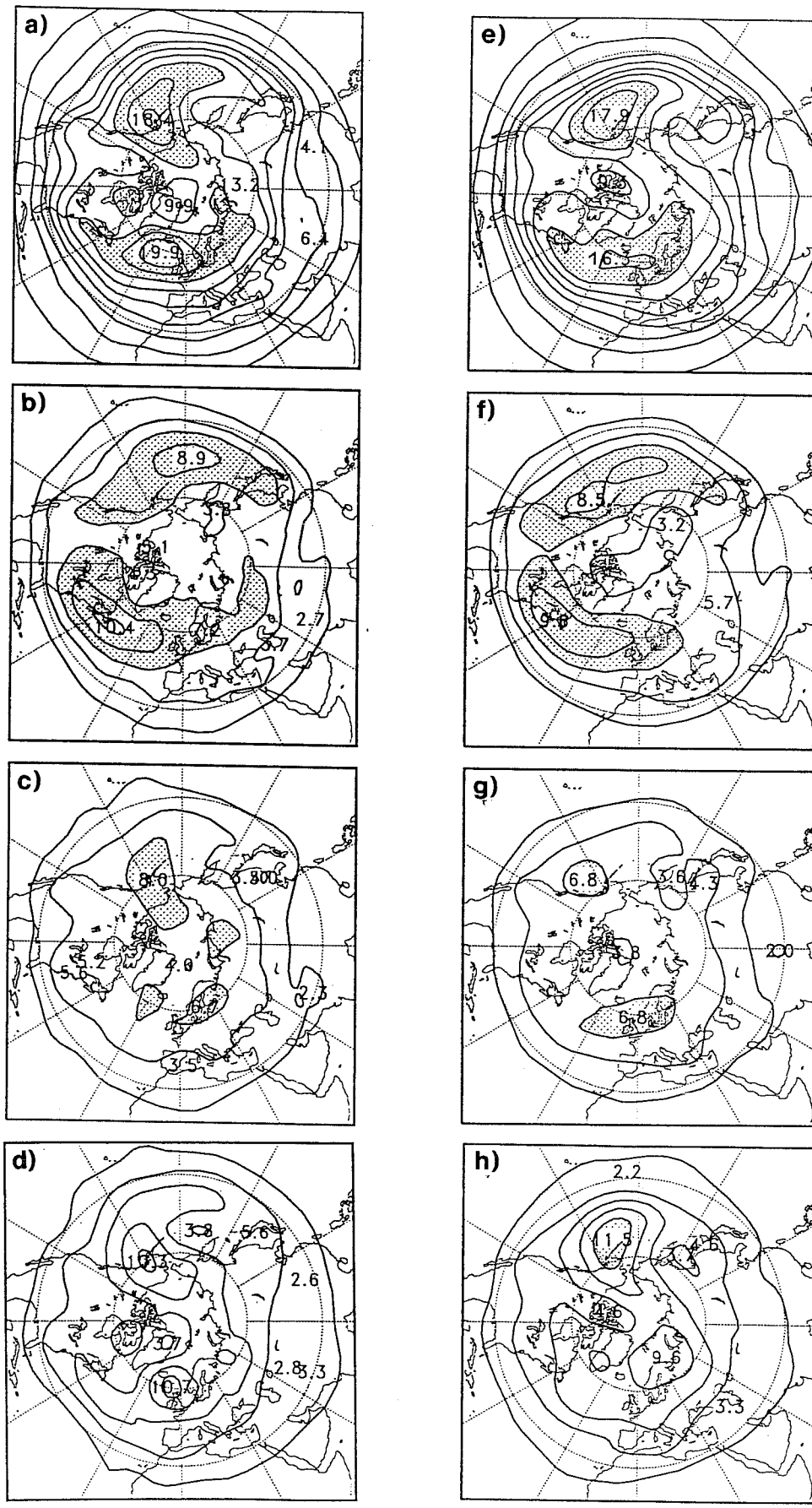

Fig.9 Standard deviation of 500 mb heights averaged for the five DJF seasons (1986/87-1990/91). Left column: analysis - a) total standard deviation, b) high-frequency band (period shorter than 10 days), c) medium-frequency band (period between 10 and 30 days), d) low-frequency band (period longer than 30 days). Right column: the same fields but for 15 model DJF simulations. Contours every 2 dam.

In the southern hemisphere the distribution of total variability is generally well represented in the model with three maxima over the southern oceans but with slightly overestimated amplitudes (not shown). The breakdown into frequency ranges shows that the model also represents relatively well the HF part of natural variability. The differences emerge in the MF range over the southern Indian ocean and especially over the southern Pacific, where the maxima in the model are shifted eastward. This is consistent with the model downstream displacement of blocking frequency maxima in the southern hemisphere as discussed by *Branković* (1992). The LF part of the model variability shows some spurious maxima which may be related to inadequate representation of tropical LF variability.

5.2 Frequency of blocking

Another useful indicator of medium-frequency variability in midlatitudes, observing the convention from the previous subsection, is frequency of blocking occurrence as defined by *Tibaldi and Molteni* (1990). Fig. 10 shows the 5-year average of the DJF and MAM 5-day filtered frequency of blocking as function of longitude for 500 mb heights in the latitudinal band between 40°N and 80°N. During the northern winter (Fig. 10a) the average frequency of the model blocking over the Atlantic/European region is comparable with the analysed, but the location of the maximum is displaced eastward. Over the Pacific the model largely underestimates the blocking frequency.

In the northern spring there are two maxima of analysed blocking frequency around the Greenwich meridian (Fig. 10b, dashed line). The main maximum is located over western Europe, and the secondary maximum is found over the eastern Atlantic. The model captured both of these peaks, however, they are of the same magnitude. In addition, the observed Atlantic minimum at 50°W has become a relative maximum in the model. One may argue, therefore, that, in contrast to the winter case, there is a tendency of simulated maxima of blocking frequency to be displaced westwards. In the Pacific region, the model again underestimates the frequency of blocking occurrences.

The fact that despite realistic boundary forcing over the oceans there is a lack of Pacific blocks in the model, may indicate the prevailing effect of upper-air circulation in generating and maintaining blocks in this region. This is indirectly confirmed by almost unchanged magnitude of the total mean error of zonal wind at 850 mb over the Pacific when compared with the mean error derived from all non-Pacific block cases, i.e. the inclusion of Pacific blocking cases does not influence significantly the amplitude of mean error (not shown). It may seem appropriate, therefore, to assume that the well known model deficiency, the intensification of the jet in the central and eastern parts of the northern Pacific and consequently the weakening of the confluence over the western coast of North America (cf. Fig. 2), are the main causes for underestimated blocking frequency over the Pacific.

Over the Atlantic/European region the performance of the model, in a statistical sense, may be regarded as relatively satisfactory, but the inconsistency in the positioning of blocking maxima in the two seasons seems puzzling. In both seasons the model generated maxima of blocking occurrences are found to be in the longitudes with relatively colder underlying temperatures when compared with the adjacent regions. By virtue of experiment design these temperatures over the Atlantic should be realistic. However, in contrast to the Pacific blocking, the 850 mb zonal wind mean error budget shows a significant contribution of the Atlantic/European blocks to the total error. These results warrant further study with the aim to explain erroneous positioning of the Atlantic/European blocking in the model simulations.

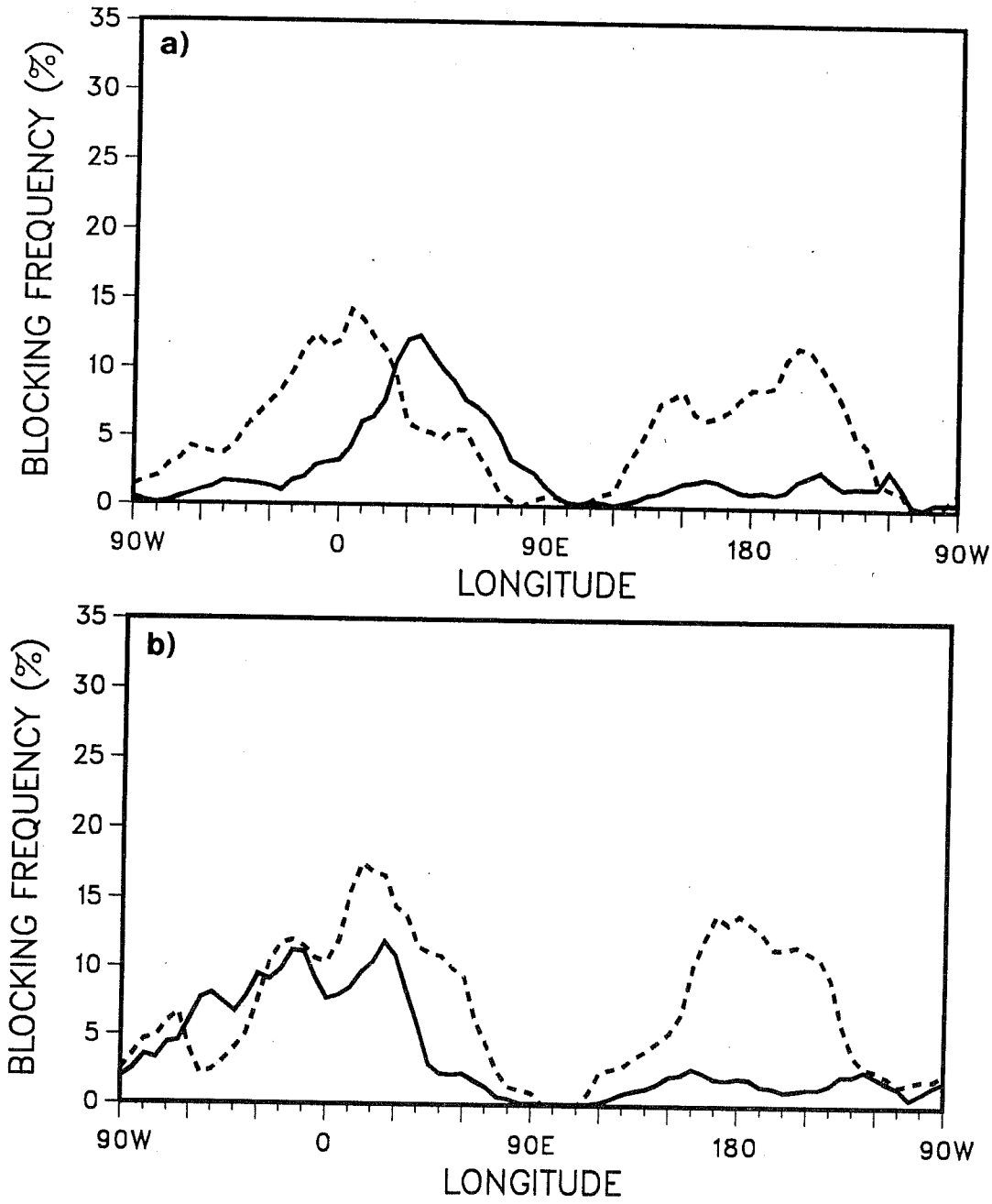

Fig.10 Mean (1986-1990) 500 mb height 5-day filtered frequency of blocking between 40°N and 80°N for a) DJF and b) MAM seasons. Solid line model, dashed analysis.

5.3 Circulation regimes statistics

In this section we investigate how well the model simulated frequency of occurrence of the most prevailing circulation regimes compares with the observation statistics. The selection of circulation regimes is based on the classification of the wintertime northern hemisphere flow patterns into clusters. The clusters have been defined for 500 mb 5-day mean geopotential eddy field using an EOF analysis. The anomaly patterns considered here are shown as the first five clusters in Fig. 12a in *Molteni et al.* (1990).

In Fig. 11 hatched bars denote observed (analysed) frequency and solid bars denote the model simulated frequency of occurrence of such defined circulation regimes. In order to establish whether the model (15 runs) can represent statistical properties of wintertime circulation regimes, the analysed frequency in Fig. 11 was derived from an ensemble of 12 winters, i.e. it does not coincide with verifying years only. This introduces some inconsistency in the SSTs between the two sets of data, however the extreme SST events (even in the short 5-winter period used for model integrations) appear to be well balanced.

For cluster 1, which characterizes the mean (climatological) winter state, the model frequency is greater than the analysis frequency. However, bearing in mind this is the most populated cluster (which contains about one third of all fields examined), such an increase in the model frequency may not be considered as a dramatic deterioration. Nevertheless, this overestimated frequency means that, on average, during winter simulations the model tends to reach the climatological state more often than the real atmosphere and therefore may imply less (medium to low frequency) variability in the model than in the analysis data.

The situation is less favourable with cluster 2 where the model estimated frequency is almost doubled when compared with the observed one. This cluster is characterized with the strongest positive PNA signature and the result indicates that the positive PNA anomaly pattern is relatively the most 'preferred' model circulation regime. The following two clusters which represent a low-wave-amplitude and a high-wave-amplitude regime respectively, show somewhat underestimated frequencies by the model. However, in spite of these reductions, the simulated frequency is proportional to the observed one, i.e. cluster 4 is less populated than cluster 3 in both observed and model frequencies. Only cluster 5, which represents a strong negative PNA pattern, shows the equal number of occurrences for both the model and analysis.

The above assessment shows that in a climatological sense the model is able to simulate and represent relatively successfully certain northern hemisphere circulation regimes. Our results may be considered, to a certain extent, as an improvement over the results for operational medium-range forecasts obtained by *Molteni and Tibaldi* (1990). The two sets of results are not directly comparable, because medium-range forecasts are strongly influenced by initial data. However, one may assume that the impact of initial data in the medium-range is 'offset' by the impact of realistic boundary forcing in the seasonal integrations. *Molteni and Tibaldi* (1990) found that an earlier T63 version of the ECMWF model substantially overestimated the frequency in cluster 1. The frequency in clusters 3 and 4 was, as in our case, underestimated; however, the ratio of observed and predicted frequencies for cluster 4 seems to be less favourable in their calculation. The seasonal integrations clearly improved the frequency in cluster 5. It is only cluster 2 where seasonal runs show a relative deterioration in comparison to an earlier version of T63 model. However, this worsening may be regarded as less important because cluster 2 is the least populated of all clusters considered. Overall, the ranking of the 5 clusters in terms of frequency is the same in the model as in the observed data.

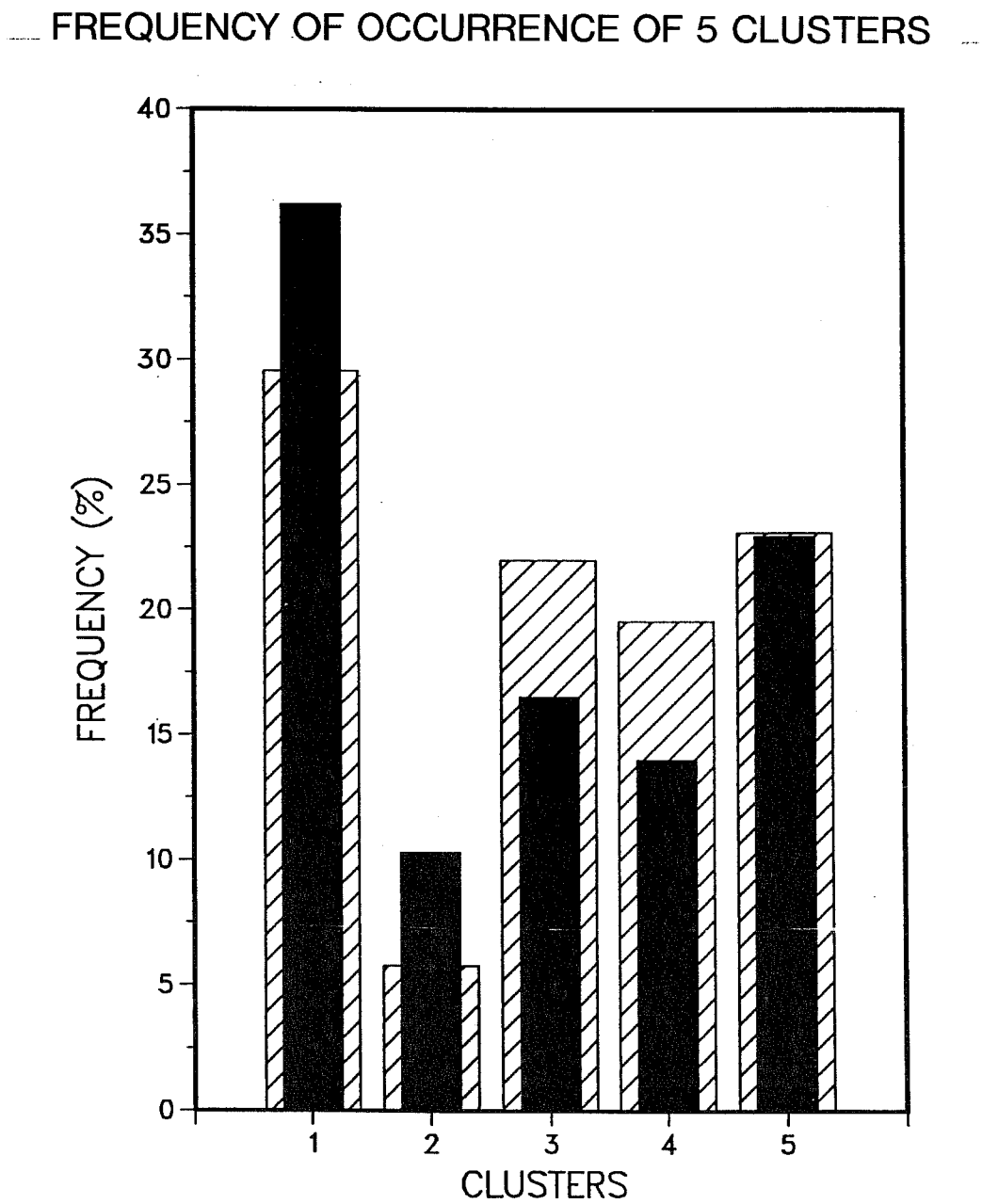

Fig.11 Frequency of occurrence of the five clusters (circulation regimes) in the DJF season: hatched bars depict analysis, solid bars 15 model integrations.

6. THE IMPACT OF MODEL FORMULATION ON SIMULATED MONSOON CIRCULATION

In order to improve operational analysis and forecasts, the formulation of ECMWF model is often changed. In this section the impact of various model formulations on monsoon rainfall during the JJA 1987 season is compared. Besides the basic cycle 36 (used in all seasonal experiments described here), one of the JJA 1987 experiments was rerun with the following model formulations: cycle 36 but with revised adjustment convection scheme (*Betts and Miller*, 1986), cycle 38 which includes modification to the surface albedo, maximum cloud overlap and revised vertical diffusion above the PBL (*Morcrette et al.*, 1991), cycle 39 which represents the major change in model dynamics by introducing the semi-Lagrangian advection scheme together with some changes in cloud parametrization (*Simmons*, 1991, *Morcrette et al.*, 1991), and finally cycle 39 but with the Eulerian formulation of advection. The semi-Lagrangian model was integrated with the same time step (22.5 minutes) as the other (Eulerian) versions.

The results of these various model formulations are shown in Fig. 12 in terms of mean JJA 1987 rainfall over the monsoon region. The reference field is 'verification' obtained from the then operational short-range forecast (Fig. 12a). It was concluded in the section on model climatology that cycle 36 produces too little rain over the Sahel and India (Fig. 12b). The cycle 38 model produces even more drying than cycle 36, particularly over the Sahel (Fig. 12d). The cycle 39 model Eulerian version (Fig. 12f), with somewhat enhanced rainfall over both India and the Sahel, improves the simulation over cycle 38, but the amounts are still insufficient when compared with Fig. 12a. The cycle 39 semi-Lagrangian version (Fig. 12e) brings the Indian rainfall amounts much closer to 'verification' but these deteriorate over the Sahel. With the adjustment scheme model cycle 36 enhances the rainfall in both regions being particularly successful in the Sahel (Fig. 12c). In addition, none of the models simulated correctly the rain shadow effect over the western Indian coast.

Fig. 13 shows analysed and simulated low-level monsoon circulation. In most of the model versions considered, a relatively pronounced southerly component along 10°S in the easterly branch of the flow is seen. This erroneous wind direction is associated with a substantial increase in low-level moisture flux convergence at the equator and consequently overestimated precipitation rates, especially in model cycles 36 and 38 (Fig. 12 b and d).

A possible explanation for such a simulated flow pattern could be the inadequate "capping" in the model of the lower tropospheric flow over the Indian ocean (M Miller, pers. comm.). The "capping" mechanism is subtly controlled by a combination of processes like large scale subsidence, entrainment and surface radiative fluxes. One of these components, the lower tropospheric vertical motion, indicates a weak subsidence at the equator in the analysis (not shown). However, in all the models this subsidence is replaced by a weak to a relatively strong ascent. This may enable the deep convection scheme(s) to become too active in regions where shallow convection should be dominant.

It is clear from the above example that due to complexity of feedbacks, and interactions of various models' physics and dynamics it is often very difficult to identify a single model feature which may be responsible for the differences discussed above. The MONEG intercomparison of the results obtained from various GCMs has shed some light on possible causes for model generated differences in monsoon circulation (*WMO*, 1992).

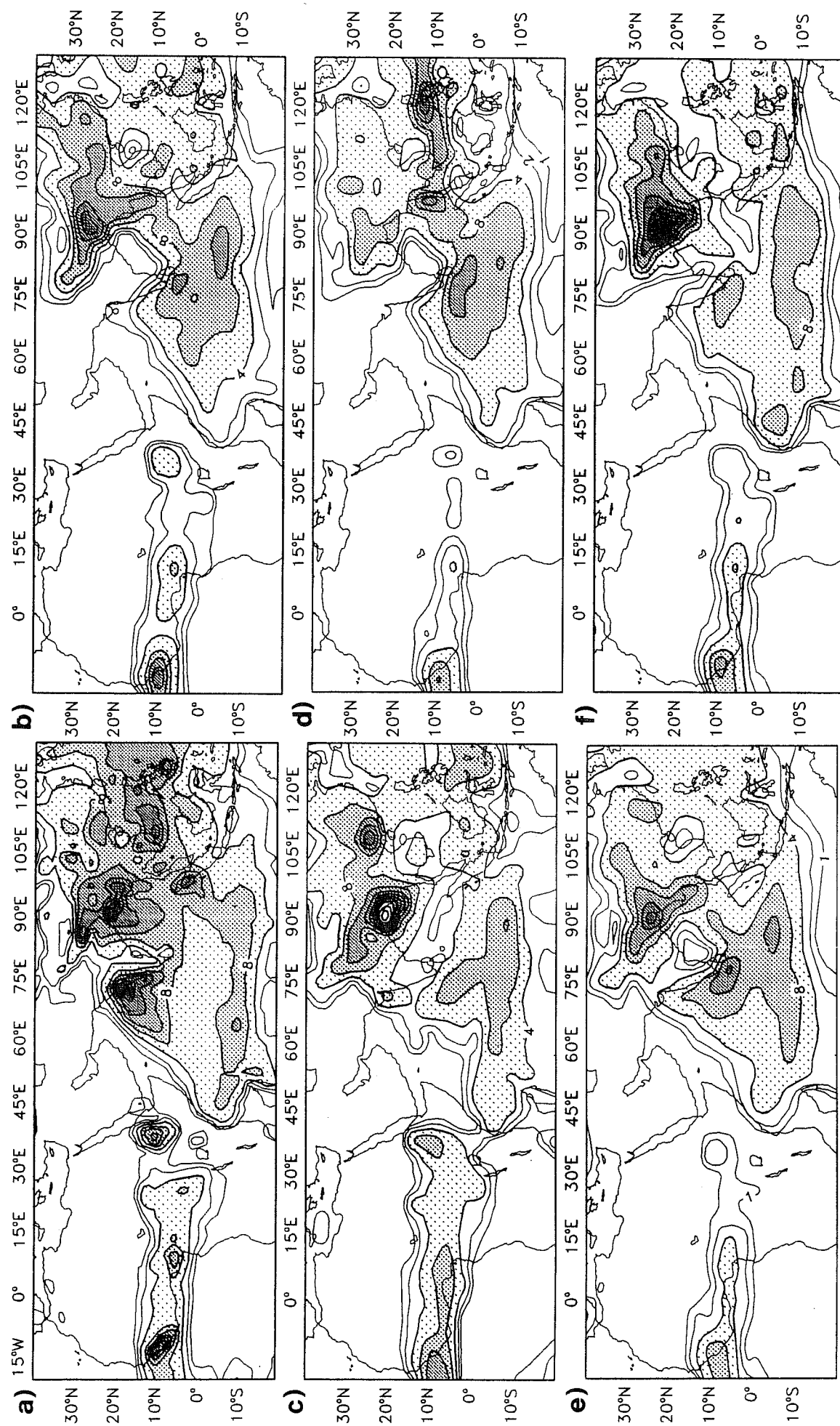

Fig.12 Mean JJA 1987 rainfall for a) ECMWF operational short-range forecast, b) cycle 36, c) cycle 36 with adjustment convection, d) cycle 38, e) cycle 39 and f) cycle 39 eulerian. Contours as Fig.4.

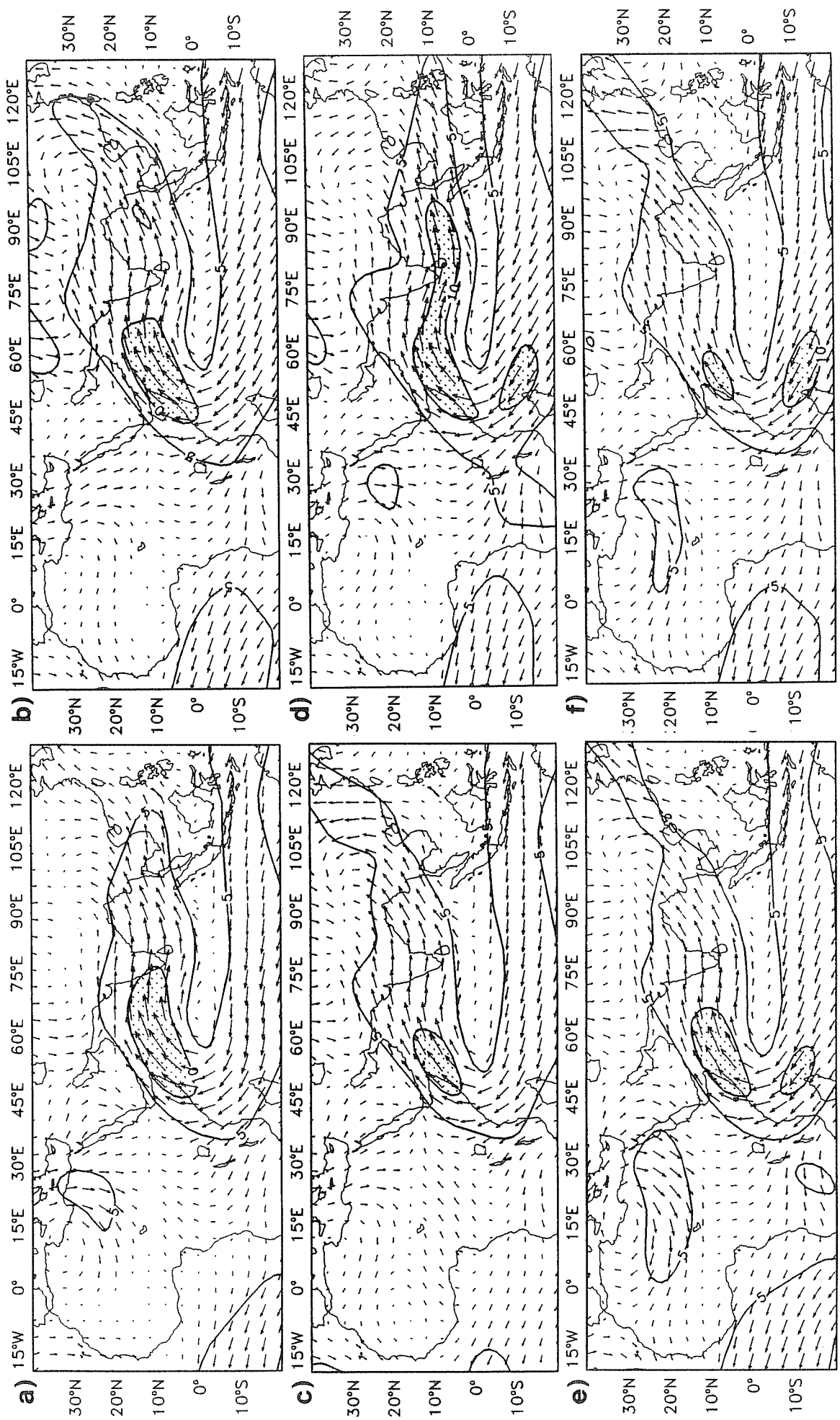

Fig.13 Same as Fig.12 but for 850 mb wind. Contours every 5 ms^{-1}.

7. PREDICTABILITY OF SEASONAL SIMULATIONS

The discussion of model results so far concentrated mainly on model ensemble mean fields, i.e. on averages obtained from three runs within a single season for a given year. It is of interest, however, to assess whether there is consistency between the simulations within the same season but initiated on consecutive days. This problem of predictability will be discussed separately for the tropics and for the extratropics.

Fig. 14 (a to c) shows the JJA rainfall anomalies over the monsoon area for experiments from 1, 2 and 3 May 1987. The consistency in pattern and amplitude of the anomaly over the Sahel and the Gulf of Guinea is striking. Over India, on the other hand, there is little similarity between the run from 2 and run from 3 May 1987. In the corresponding JJA 1988 individual experiments (Fig. 14 d to f) a consistent model response to SST forcing is seen again over the Sahel, whereas over India a less coherent pattern emerges. Similar results are also found in other JJA seasons.

The results for the African tropical strip indicate relatively strong predictability and they are certainly encouraging bearing in mind the problem of drought and crop production in the Sahelian countries. The inconsistency in model response over India may indicate inherent predictability problem for the region. However, in view of the discussion of the results of Figs. 12 and 13, a possible modelling problem should not be discounted.

In Fig. 15 we consider the impact of two different La Niña anomalies, one with very pronounced amplitude (DJF 1988/89) and one with a weak amplitude (DJF 1989/90), on the model extratropical height field. In the PNA region, the upper-air response to a strong equatorial Pacific SST forcing (Fig. 15 a to c) is relatively consistent in all experiments initiated on consecutive days and takes the shape of a negative PNA teleconnection pattern. (This agrees well with observed anomaly field.) In the northern hemisphere, away from the PNA region, corresponding anomalies from different experiments tend to disagree and become rather dispersed. Over Europe, for example, each experiment has generated a different type of anomaly with no resemblance to each other. It is interesting to note that in the southern hemisphere a significant and similar pattern emerges in all experiments. It could be said that the southern hemisphere pattern tends to be a "mirror image" of the La Niña impact on the model northern hemisphere extratropics.

Results similar to these are obtained for a strong El Niño forcing in DJF 1986/87, i.e. model response in the PNA region was consistent in all individual runs, and a less coherent picture is seen in other regions of the world. Of course, anomaly pattern was typical of a positive PNA teleconnection pattern.

With a weak La Niña (Fig. 15 d to f) height anomalies vary significantly from one experiment to another. Even in the PNA region anomalies with the opposite sign are found. In the southern hemisphere the model response is rather weak. In other years, with a weak Pacific SST anomalies, no regular pattern emerges and the model response was in terms of prevailing disorganized anomalies.

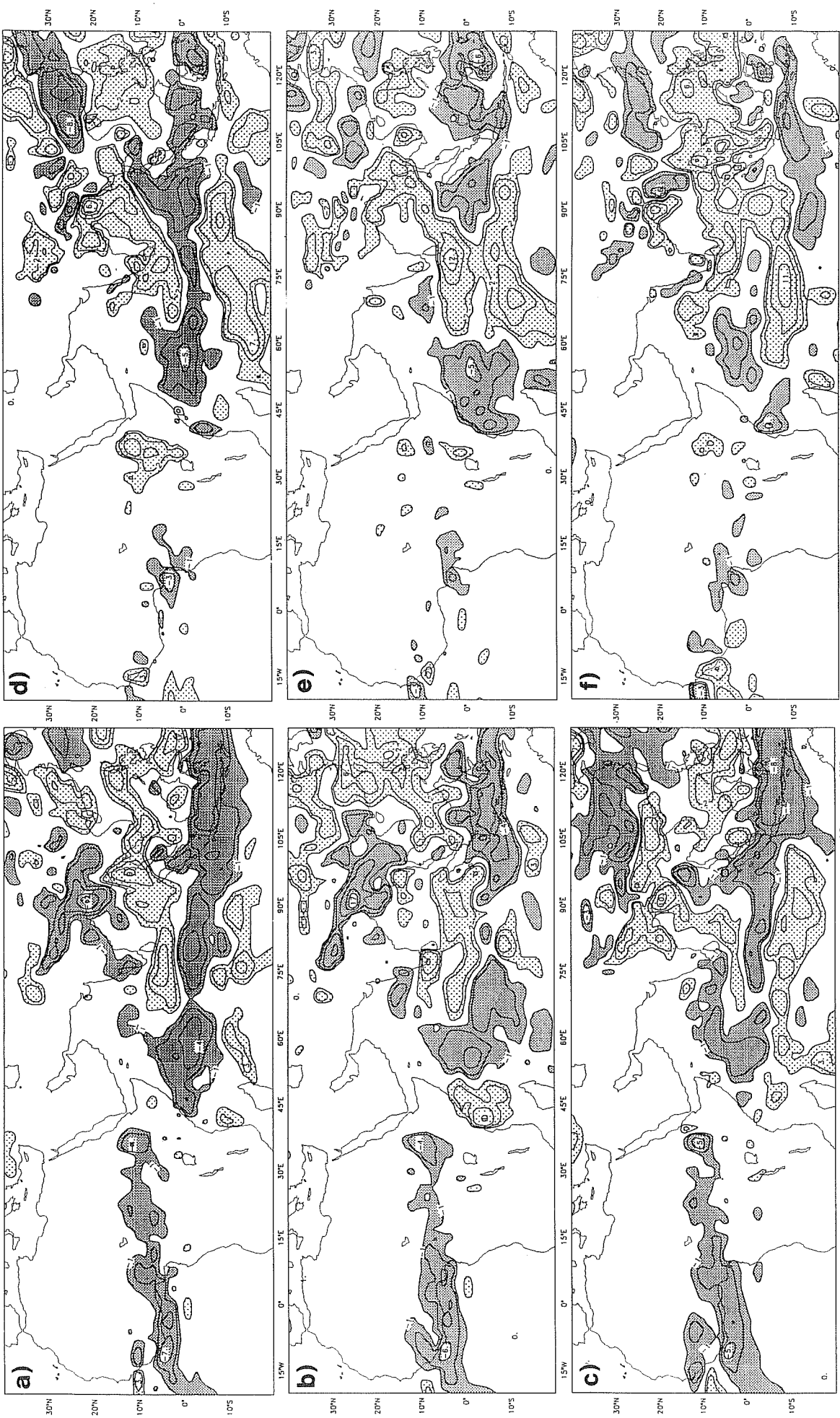

Fig.14 JJA rainfall anomalies for experiments initiated on a) 1 May 1987, b) 2 May 1987, c) 3 May 1987, d) 1 May 1988, e) 2 May 1988 and 3 May 1988. Contours as Fig.7.

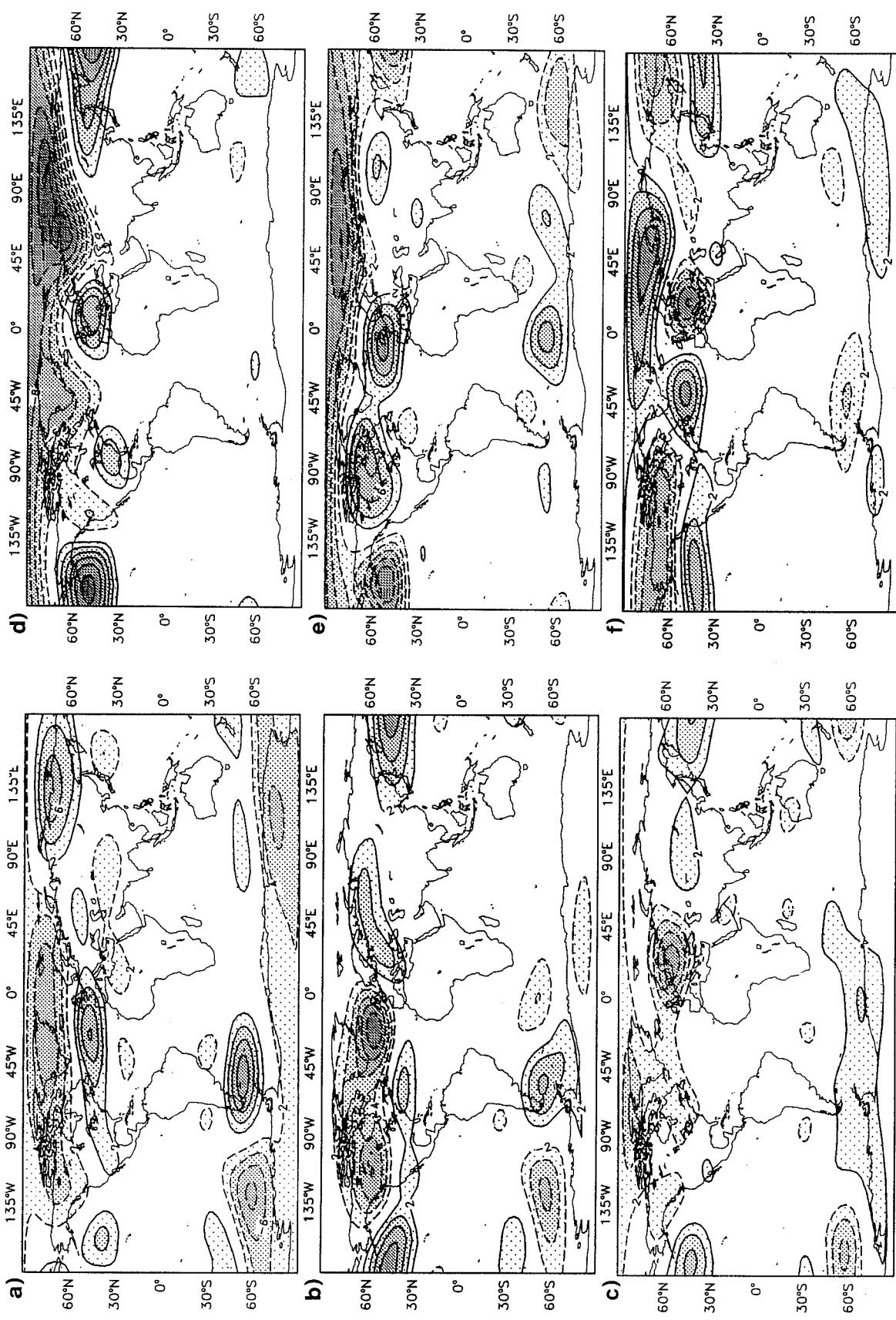

Fig.15 DJF 500 mb height anomalies for experiments initiated on a) 1 November 1988, b) 2 November 1988, c) 3 November 1988, d) 1 November 1989, e) 2 November 1989 and f) 3 November 1989. Contours every 2 dam.

8. CONCLUSIONS

The two model simulated seasons JJA (June, July, August) and DJF (December, January, February) have been analysed from a comprehensive set of 120-day integrations with a T63 version of the 1990/91 ECMWF numerical weather prediction model. For each season, over the period of five years (1986-1990), three integrations initiated on consecutive days were run. In all experiments observed sea surface temperatures (SSTs) were used which were updated every five days in the model.

The model seasonal climate, averaged from 15 runs for each season, reproduces the major large-scale circulation features reasonably well. Although, the zonalization of planetary waves is still evident, the positioning of semi-permanent surface lows is correctly simulated. On the regional scale, the monsoon flow is somewhat weaker in the model than observed. The monsoon rainfall amounts are lower in comparison with 'verifying' operational short-range ECMWF forecasts; however the overall tropical rainfall pattern is well captured.

The interannual variability of large-scale tropical flow is well represented in model simulations. This is true for the extratropics as well, but mainly when the equatorial Pacific SSTs anomalies are strong. The coherent and consistent model response is then primarily seen in the Pacific/North Atlantic (PNA) region. In other regions, the pattern and amplitude of model anomalies may vary. In the case of weak SST anomalies the response may differ even in the PNA region. The interannual variability in monsoon rainfall is also well simulated over the African tropical belt. However, in some regions (India) this is only a partial success.

Though the overall variability in the model agrees reasonably well with the observed variability, the breakdown into three different frequency bands (high, medium and low) reveals that contributions of these bands differ over some regions in the model from those found in the analysis.

In both DJF and MAM seasons, the model substantially underestimates the frequency of blocking occurrence in the Pacific region. This is probably related to the too strong Pacific jet and weakened diffluence over North America in the model. In the Atlantic/European region the frequency of blocking is correctly represented but the maximum is displaced towards cooler underlying temperatures.

The model is able to represent relatively successfully selected northern hemisphere wintertime circulation regimes. The frequency of the most populated cluster (climatological mean) is overestimated by the model, which may indicate its tendency to reach the climatological state more often than the real atmosphere. The frequency of the cluster with a strong positive PNA pattern is found to be doubled in seasonal simulations, whereas the frequency of the cluster with a strong negative PNA signature is well captured.

The influence of various model formulations on seasonal integrations is assessed in terms of monsoon circulation and rainfall. It was found that the model with the adjustment convective scheme reduces the dry bias over both India and the Sahel, and the model with semi-Lagrangian advection scheme improves the rainfall over India but not over the Sahel. An overestimated moisture flux convergence in the equatorial Indian ocean, and consequently increased rainfall rates, may be, at least partly, caused by inadequate simulation of vertical motion.

From experiments initiated on successive days, the predictability of seasonal averages was studied. The impact of initial data on the Sahelian rainfall was found to be relatively small. However, this is not the case over India, where rainfall amounts may have a stronger dependence on initial conditions.

A consistent upper-air response in the PNA region, when the model is forced by a strong equatorial Pacific SST anomalies, indicate a relative independence of model simulations on initial data in that region. However, even with a strong ENSO cycle, the model generates variable anomaly patterns in other parts of the globe. This may imply that the influence of the equatorial Pacific SSTs in the model is mainly felt in the immediate downstream region (possibly in both hemispheres). In the case of weak tropical Pacific anomalies the impact of initial conditions is becoming increasingly important and can offset possible influence of lower boundary forcing. These results support the notion that even for seasonal time scales multiple integrations are needed in order to better extract a signal from the noise and to overcome the influence of inherent atmospheric instabilities. Thus, a Monte Carlo approach might be seen as a viable strategy used in assessing model simulations on seasonal time scales.

Acknowledgement The authors thank Tim Palmer, Martin Miller and Franco Molteni for useful discussions and comments.

REFERENCES

Arpe, K., 1990: Impacts of changes in the ECMWF analysis-forecasting scheme on the systematic error of the model, pp 69-114 in Proceedings of the ECMWF Seminar 'Ten years of medium-range weather forecasting', Reading, UK, 4-8 September 1989.

Bengtsson, L., 1991: Advances and prospects in numerical weather prediction. Q.J.R.Meteorol.Soc., **117**, 855-902.

Betts, A.K. and M.J. Miller, 1986: A new convective adjustment scheme. Part II: Single column test using GATE wave, BOMEX, ATEX and arctic air-mass data sets. Q.J.R.Meteorol.Soc., **112**, 693-709.

Branković, Č., 1992: On seasonal simulations with the ECMWF model. Proceedings of the 3rd BMRC Workshop on Modelling Weather and Climate, Melbourne, Australia, 27-29 November, 1991.

Gill, A.E., 1980: Some simple solutions for heat-induced tropical circulations. Q.J.R.Meteorol.Soc., **106**, 447-462.

Horel, J.D. and J.M. Wallace, 1981: Planetary-scale atmospheric phenomena associated with southern oscillation. Mon.Wea.Rev., **109**, 813-829.

Jaeger, L., 1976: Monatskarten des Niederschlags für die ganze Erde. Berichte des Deutschen Wetterdienstes, **139**, Band 18.

Miller, M.J., A.C.M. Beljaars and T.N. Palmer, 1992: The sensitivity of the ECMWF model to parametrization of evaporation from the tropical oceans. J.Climate, **5**, (to appear).

Miyakoda, K., T. Gordon, R. Cavelry, R. Stern and J. Sirutis, 1983: Simulation of blocking event in January 1977. Mon.Wea.Rev., **111**, 2363-2401.

Molteni, F. and S. Tibaldi, 1990: Regimes in the wintertime circulation over northern extratropics. II: Consequences for dynamical predictability. Q.J.R.Meteorol.Soc., **116**, 1263-1288.

Molteni, F., S. Tibaldi and T.N. Palmer, 1990: Regimes in the wintertime circulation over northern extratropics. I: Observational evidence. Q.J.R.Meteorol.Soc., **116**, 31-67.

Morcrette, J.-J., L. Illari, E. Klinker, H. Le Treut, M. Miller, P. Rasch and M. Tiedtke, 1991: Clouds and radiation. ECMWF Tech.Memo. 181.

Nicholson, S.E., 1985: Sub-Saharan rainfall 1981-84. J.Climate and Appl.Meteor., **24**, 1388-1391.

Palmer, T.N., 1987: Modelling low-frequency variability of the atmosphere, pp 75-103 in Atmospheric and oceanic variability, Ed. H. Cattle, Royal Meteorological Society.

Palmer, T.N., C. Branković, P. Viterbo and M.J. Miller, 1992: Modelling interannual variations of summer monsoons. J.Climate, **5**, (to appear).

Reynolds, R.W., 1988: A real-time global sea surface temperature analysis. J.Climate, **1**, 75-86.

Reynolds, R.W. and L. Roberts, 1987: A global sea surface temperature climatology from in situ, satellite and ice data. Trop.Ocean-Atmos. Newsletter, **37**, 15-17.

Shukla, J., 1981: Dynamical predictability of monthly means. J.Atmos.Sci., **38**, 2547-2575.

Simmons, A., 1991: Development of a high-resolution semi-Lagrangian version of the ECMWF forecast model. ECMWF Tech.Memo. 180.

Simmons, A.J., D.M. Burridge, M. Jarraud, C. Girard and W. Wergen, 1988: The ECMWF medium-range prediction models: Development of the numerical formulations and the impact of increased resolution. Meteorol.Atmos.Phys., **40**, 28-60.

Tibaldi, S. and F. Molteni, 1990: On the operational predictability of blocking. Tellus, **42A**, 343-365.

WMO, 1991: Extended abstracts. ICTP/WMO International Technical Conference on Long-Range Weather Forecasting Research, Trieste, Italy 8-12 April 1991. Long-Range Forecasting Research Report No.14, WMO/TD No.395.

WMO, 1992, Report of the third session of the monsoon numerical experimentation group. (to be published)